Scientific Research Publishing

Open Journal of Fluid Dynamics, 2022, 12, 249-262
https://www.scirp.org/journal/ojfd
ISSN Online: 2165-3860
ISSN Print: 2165-3852

Formation of Gel-Like Shear-Induced Structure with Dosing of Dilute Surfactant Solution and Its Effect on Turbulent Channel Flow

Shumpei Hara[1], Kazuki Ishii[2], Yasuo Kawaguchi[2]

[1]Department of Mechanical Engineering, Doshisha University, Kyoto, Japan
[2]Department of Mechanical Engineering, Tokyo University of Science, Chiba, Japan
Email: shhara@mail.doshisha.ac.jp

How to cite this paper: Hara, S., Ishii, K. and Kawaguchi, Y. (2022) Formation of Gel-Like Shear-Induced Structure with Dosing of Dilute Surfactant Solution and Its Effect on Turbulent Channel Flow. *Open Journal of Fluid Dynamics*, **12**, 249-262.
https://doi.org/10.4236/ojfd.2022.123012

Received: June 9, 2022
Accepted: July 29, 2022
Published: August 1, 2022

Abstract

A shear-induced structure (SIS) is formed under appropriate concentration and shear conditions in a surfactant micellar solution. In this study, we performed experiments of surfactant solution dosing in a fully developed two-dimensional turbulent channel flow from a sintered metallic wire mesh plate attached to a side wall. We investigated the behavior of the solution under the elongation during its passing through the wire mesh and under the strong shear due to the channel flow. It was confirmed that the dosed solution containing a laser dye was visualized by a laser sheet, and the accumulated gel from the wire mesh formed a layer and developed with time. Consequently, on dosing the dilute surfactant solution from the wire mesh, a gel-like SIS layer was formed, which majorly covered the wire mesh plate. The gel-like SIS layer on the wire mesh plate acted as a sticky solid and restricted the flow in the channel. This layer continued to grow while dosing, owing to which the pressure drop of the channel flow significantly increased. The gel-like SIS layer grew rapidly even in the turbulent flow and reached the equilibrium thickness. After the termination of the dosing, the gel layer collapsed gradually. In addition, the thickness of the gel-like SIS layer (indicating the strength indirectly) strongly depended on the surfactant concentration and the elongation rate in the wire mesh.

Keywords

Turbulent Channel Flow, Viscoelastic Fluid, Gelation, Scalar Transfer, PIV/PLIF

1. Introduction

Sol-gel characteristics that respond to a wide variety of stimuli have been the focus of numerous previous studies [1]-[7]. In a surfactant solution categorized as a viscoelastic fluid, shear induces sol-gel characteristics with a change in the volume. Shear-induced structures (SISs) in long wormlike micelles are formed locally in the flow of the surfactant solution [8]. Chu *et al.* [9] reported that gelation occurred simultaneously with the transition to shear-banding. Yamamoto *et al.* [10] observed the simultaneous appearance of turbidity and SISs, shear-banding, and stress fluctuation (a phenomenon in which the viscosity fluctuates in a long cycle of the rheometer). These reports suggest that shear-banding is closely related to SISs and gel formation [11]. Furthermore, a surfactant solution containing the formed SISs reduces the wall friction under turbulent flow conditions. Such a solution is expected to be used for energy saving in an air conditioning equipment, which circulates hot and cold water, and in district cooling and heating systems. This is because the surfactant solution has the characteristic of restructuring against the destruction of the micellar structure caused by the strong shear from the flow. Particularly, when a counter ion is added to a cationic surfactant solution, stable wormlike micelles are formed even at a dilute concentration. They provide the solution with remarkable viscoelasticity, which is essential for its drag-reducing ability. Thus, the surfactant solution has been studied in various basic research fields. In numerous previous studies, thus far, SISs were treated as dispersions; however, in the study of an impinging wall jet flow, Tuan *et al.* [12] reported that gel-like SISs acted similar to the lumps of soft gels in the liquid confining the flow around a jet. Moreover, Vasudevan *et al.* [13] presented that a surfactant micellar solution formed an irreversible gel in an elongation-dominated microchannel flow, and it maintained the gel state even after 20 months. Under the condition of a microfluidic flow, some reports presented the microstructure of the flow-induced structural phase in worm-like micellar solutions [14] [15]. There are also references to the passage of non-Newtonian nanofluids through porous media [16] [17].

However, there is no report on the prediction of the formation of gel-like SISs and about the persistence of the condition in which a high shear is induced by a high-speed flow. In living bodies, the high-speed flows in large animals (such as in arteries) and the flows with high stress in the digestive tract are controlled by soft materials, such as blood vessel walls, valves, and the digestive tract. Gels play a key role in the drag reduction on the slimy skin surface of an organism, such as fish, allowing it to move efficiently in water [18]. They are also types of soft materials important in the industrial field [13] [19] [20] [21]. If a gel-like SIS can be formed under a high-speed flow condition with a strong shear, then applications in the field of biomimetics can be expected in the future. Previous studies focused on the injection of a mucus, polymer, or surfactant in the wall vicinity or on the wall [18] [22] [23] [24] [25]. However, they did not consider the possibility of gel formation in turbulence and of diffusion of the gel to the flow.

The present study aims to characterize a gel-like SIS formation for dosing a surfactant solution in the channel flow from a permeable wall attached to a side wall. The permeable wall elongates when the solution passes through the wire mesh, whereas shear deformation is caused by the channel flow of the solution. In this flow, we can observe the exposure to a transverse force and a high shear; however, the possible occurrence of gel formation is still unknown. It is found that if a gel-like SIS has sufficient strength to be attached to a wall, the gel narrows the channel flow area, and it can also be used as a soft-material valve.

This paper is organized as follows. In Section II, the experimental configuration of the channel flow with the dosing system, pressure loss measurement, particle image velocimetry (PIV), and planar laser-induced fluorescence (PLIF) measurements are presented. In Section III, the characteristics of the gel-like SIS formed in the channel flow after reaching the equilibrium state are described based on the PLIF visualization and the PIV measurement. In Section IV, the temporal growth process of the gel-like SIS layer is discussed in terms of the change in its thickness with continuous dosing and after stopping the dosing. In Section V, the relation between the blocking extent and the boundary condition of the stress on the gel-like SIS layer is discussed based on the pressure loss measurement. In Section VI, we examine the influence of elongational deformation on the thickness of the gel-like SIS layer. Finally, a summary of the main conclusions is presented.

2. Experimental Set-Up and Conditions

The experiments were conducted in a closed-circuit channel flow, as displayed in Figure 1. A part of the channel is a two-dimensional acrylic channel with a total length of 6000 mm, a channel height of 40 mm (=2*h*), and a channel width of 500 mm (=25*h*). To dose the surfactant solution, three permeable walls are installed on a 1450-mm side wall, in a part of the above-mentioned two-dimensional

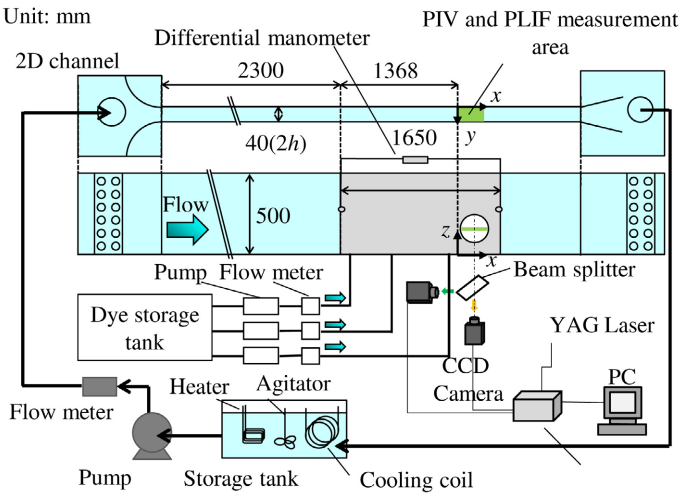

Figure 1. Schematic overview of the experimental set-up in the pressure loss measurement, PIV and PLIF measurements.

channel. The leading edge of the permeable section is located 2300 mm (=115h) downstream from the channel inlet, and a fully developed flow is observed at this location. The porous wall is made by laminating and sintering seven mesh sheets (#50 + #100 + #40 + #20 + #40 + #100 + #50). The wire mesh on the surface of the permeable wall directly facing the channel flow has 0.32 mm opening width and 0.19 mm wire mesh diameter. The origin of the coordinate system, in which x is the streamwise direction and y in the wall-normal direction, is located at the center of the leading edge of the permeable section. The dosing fluid in the small tank is supplied to the permeable section by three-roller pumps.

The bulk mean velocity, U_b, was estimated by the cross-section area (40 mm × 500 mm) and by the flow rate measured by an electromagnetic flow meter located upstream of the two-dimensional channel. In the pressure loss measurement, the pressure difference, Δp, between two taps L-distance apart present across the permeable section was measured with a precise differential pressure gauge. Visualizations by the PLIF and PIV measurements were conducted with a sheet-like laser by double-pulse irradiation and a CCD camera in the x-y plane on the permeable plate, sufficiently downstream, *i.e.*, 1368 mm (68.4h) from the leading edge. To identify the dosing fluid and bulk flow in the channel, a fluorescent dye (Rhodamine WT) was added to the dosing fluid. This allowed tracking of the dosing fluid from the permeable wall in the visualized image. The PIV tracer particles were nylon powder with an average particle size of 4.1 μm.

A dilute cationic surfactant solution of cetyltrimethylammonium chloride (CTAC) prepared with the same weight concentration of sodium salicylate (NaSal) as the counter ion was employed at a constant temperature of 298 ± 0.2 K achieved by a heater and a cooling coil. The experiment was performed with five selected surfactant concentrations: 0 ppm (water) for reference, 25, 40, 80, and 150 ppm.

In the experiment, the surfactant concentrations in the channel fluid and dosing fluid were varied in each case. We named the experimental cases for each solution combination, as summarized in Table 1. To identify the differences between the water and dilute surfactant solution flows at the same U_b, the Reynolds number was defined as $\mathrm{Re} = 2U_b h/\nu$, based on the kinematic viscosity of water, ν. The Reynolds number of the channel flow was fixed as $\mathrm{Re} = 1.0 \times 10^4$.

Table 1. Surfactant concentration of fluids in experimental cases.

Case	Fluid of channel flow	Dosing fluid
W-W	0 ppm (Water)	0 ppm (Water)
W-C150	0 ppm (Water)	150 ppm
C25-C25	25 ppm	25 ppm
C40-C40	40 ppm	40 ppm
C80-C80	80 ppm	80 ppm
C150-C150	150 ppm	150 ppm

To eliminate the kinetic influence of the dosing itself on the turbulent channel flow, we gradually dosed the surfactant solution. The dosing velocity, U_d, was varied from 2.0×10^{-4} to 8.0×10^{-4} m/s. This corresponds to the dosing ratio of $U_d/U_b = 8.9\times10^{-4}$ - 3.6×10^{-3}. In the PLIF and pressure loss measurements, the dosing continued at a constant flow rate up to 600 s of the elapsed time, t, following which, it was immediately stopped to investigate the process of the growth and collapse of the gel layer. This testing process corresponded to the opening and closing operations of a valve using a soft material [26].

3. Characteristics of Gel-Like SIS Layer in Equilibrium State

3.1. Visualization of Gel-Like SIS Layer

We performed the experiments of dosing the surfactant solution in the channel flow from the permeable wall, to form a layer of a gel-like SIS. PLIF measurements were initially performed to visualize the formation of the gel-like SIS and to determine its thickness. Figure 2 displays the images obtained via the PLIF visualization in three experimental cases for different combinations of dosing of water and a 150-ppm surfactant solution as a typical case. The vertical and the horizontal axes of the image are normalized with the channel half-height, h. In the image, the white areas generated by the strong scattered light of the dye indicate a high dye concentration. Thus, the image represents the spatial distribution of the dosing fluid. When the dosing fluid becomes gel-like, it can be confirmed that the light scattering area illuminated by the laser sheet remains close to the wall in a layered state.

For the W-W case, the high dye concentration rapidly diffuses toward the channel center from the permeable wall because of the high diffusivity of the Newtonian fluid turbulence. In contrast, for the C150-C150 case, the white (high-dye concentration) area, which is different from that for W-W case, is distributed as y/h = 1.5 (30 mm) in the y direction. Furthermore, the white area vibrates but remains attached to the wall. The magnitude of the streamwise velocity in this region is approximately equal to zero, in the results of the PIV velocity measurements, as explained subsequently. There is a flow and shear stress, except for in the white layer, which can sustain the shear stress, although there is

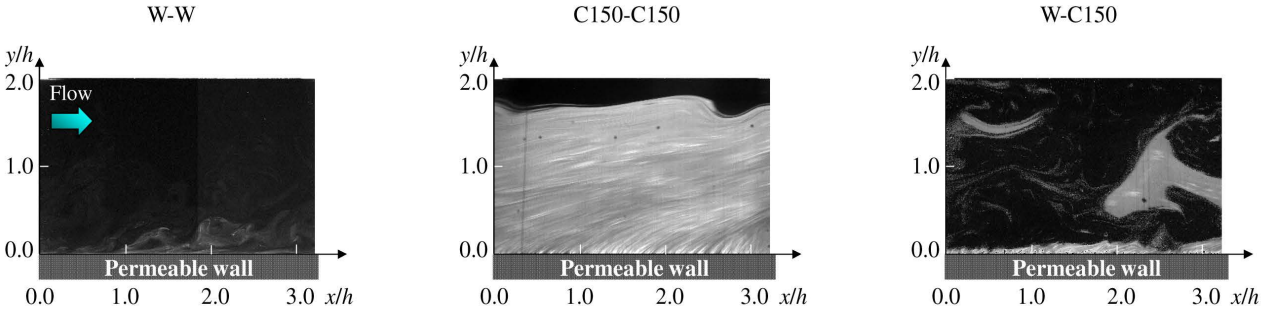

Figure 2. Typical PLIF images at t = 500 s for the case of different combinations of dosing into a fully developed channel flow at $U_d = 2.0 \times 10^{-4}$. The brightness on the images corresponds to the dye concentration.

no flow in it. Therefore, it can be concluded that this layer on the permeable wall is solid and sticky. This layer formed by passing through the permeable wall is named the gel-like SIS layer.

Additionally, the gel-like SIS includes numerous stripes, which are inclined close to the dosing wall and further toward the downstream direction in the outer region. The x-directional spacing of the gel-like SIS stripes corresponds to the pore distance in the mesh of $0.026h$. From these results, it is concluded that initially gel-like SISs are formed from each pore of the permeable mesh wall in a thread shape, which then merge with increasing y-direction. For the case of W-C150, a gel-like SIS layer is observed on the thin white layer from the permeable wall, despite the transverse flow and the high shear in the wall vicinity resulting from the dosing to the Newtonian turbulence. Numerous filamentous gels of high-dye concentrations occasionally broke away from the gel layer because of the high shear and the high diffusivity in the outer water flow.

Figure 3 exhibits the dependency of the gel-like SIS layer in the PLIF images on the surfactant concentration. In addition to the case of C150-C150, cases of C40-C40 and C80-C80 exhibit the gel-like SIS layer with stripes. The gel-like SIS sticks to the permeable wall, and its thickness increases remarkably with the increase in the surfactant concentration. However, in the case of C25-C25, the dosing fluid is flowing with no stripes near the wall, and therefore, the gel-like SIS is not developed because the very dilute concentration is under a critical value. However, the image exhibits a general drag reduction flow with a low diffusivity, leading to a dense dye concentration area caused by the suppressed turbulence. From these results, it was found that gel-like SISs significantly develop from the permeable wall, even in the channel turbulent flow if the conditions, such as the surfactant concentration, are suitable.

3.2. Velocity Distribution in Channel Flow Obtained by PIV Measurements

The velocity distribution in the x-y plane in the channel was measured by the PIV system. When a solid-like layer is formed, the streamwise mean velocity is 0 in the region of the gel and a flow is observed in the other regions of the channel. The streamwise mean velocity was calculated by averaging 500 pairs of PIV images when the growth of the gel-like SIS reaches equilibrium. The measurements

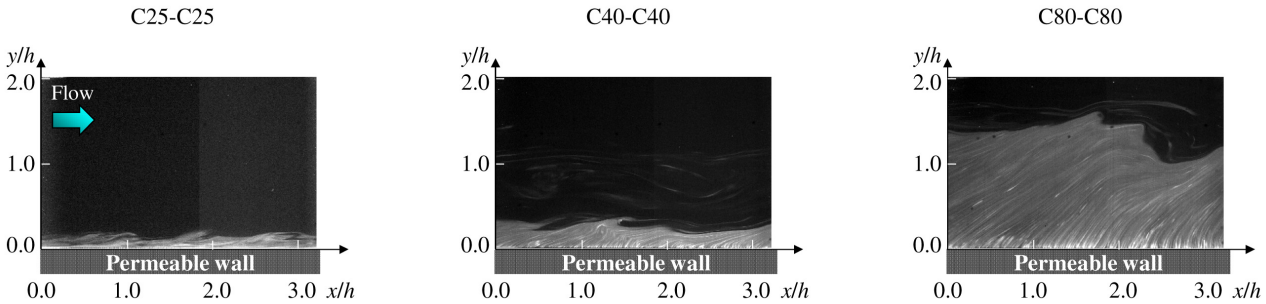

Figure 3. Typical PLIF images at $t = 500$ s for the case of various surfactant concentrations at $U_d = 2.0 \times 10^{-4}$.

confirmed that the flow rate of the channel flow measured by the electromagnetic flow meter was unaffected by the growth of the gel-like SISs. The streamwise mean velocity, $\bar{U}$, profile normalized with the outer scale (U_b and h) in the wall-normal direction is displayed in Figure 4.

For the cases of W-W and C25-C25, the velocity distributions are symmetrical in the $y/h = 1$ plane, and there is no indication of the growth of a solid-like gel layer from the wall, at $y/h = 0$. For the case of C25-C25, the central portion of the velocity distribution protrudes, resulting in a typical drag-reducing flow velocity distribution. However, the cases of C40-C40, C80-C80, and C150-C150 exhibit completely different characteristics. Because the gel-like SIS layer sticks on the permeable wall located at $y/h = 0$, there is a zone with a streamwise mean velocity of 0. Furthermore, for the high concentration cases of 80 and 150 ppm, this layer is still sticky on the permeable wall, even when the thickness in the y direction increases to $1.5h$ or more. This result indicates that the gel-like SIS layer is like a solid and is not peeled off aggressively by the turbulent flow flowing on the upper surface of the layer.

4. Temporal Growth Process of Gel-Like SIS Layer

To investigate the growth and collapse processes of the gel-like SIS layer, the acquisition of the images was started simultaneously with the start of dosing, and the acquisition was continued for some time even after the dosing was stopped. The typical acquisition duration was 1200 s. Image analysis was performed on each of the 600 visualized images to calculate the gel layer thickness in the temporal transition. It is noted that the image analysis is conducted only for the cases in which a gel-like SIS layer is formed. Therefore, the data for the case of C25-C25 are excluded from the figure, because a gel-like SIS formation was not confirmed in all the visualized images, PIV measurement, and pressure loss measurement, as explained subsequently.

First, the binarization for the image was performed based on the threshold of the brightness of the gel-SIS layer. The binarized value was defined as $C(x, y)$. Because the surface of the gel layer was wavy, the binarized values were averaged on the x-direction to determine the average thickness in the image. Second, the

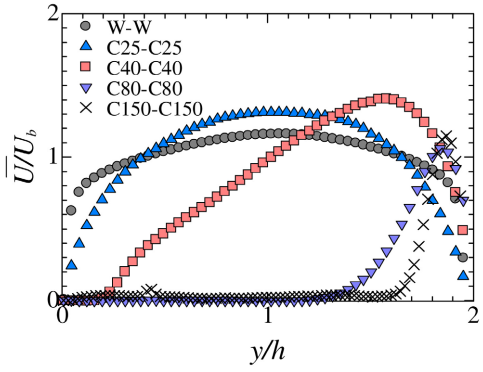

Figure 4. Streamwise mean velocity profile at $U_d = 2.0 \times 10^{-4}$.

layer thickness of the gel-like SIS, H_g, was defined as the y position corresponding to $\overline{C(y)} = 0.5$, *i.e.*, the wave intermediate height at which the gel layer and the channel fluid exist in the same proportion at a constant y line.

The temporal transition of the thickness of the gel layer for various surfactant concentrations is presented in Figure 5. The horizontal axis is the elapsed time, t, from the start of the dosing, and the vertical axis is the thickness of the gel layer normalized by h. In Figure 5, the record starts at t = 0 s with the start of the dosing, and the dosing is stopped at t = 600 s. The recording is continued until t = 1200 s, to analyze the process of the collapse of the gel layer. At all the surfactant solution concentrations, the thickness rapidly increases based on the elapsed time from the start of the dosing. Subsequently, the increase rate decreases from approximately t = 200 s. This is because the channel flow is restricted by the gel layer and the mean velocity increases with the growth of the layer, which results in activation of the gel layer destruction. The thickness of the gel layer becomes steady when the gel formation from the permeable wall and the destruction from the channel flow reach an equilibrium state. Furthermore, it can be confirmed that the gel-like SIS layer is destructed, and its thickness decreases gradually after the dosing is stopped at t = 600 s. The gel layer does not disappear instantly after 600 s, and it is sticky on the permeable wall under this shear condition. These tendencies are observed for all the dosing velocity conditions, as presented in Figure 5. In addition, the thicknesses for cases C80-C80 and C150-C150 exhibit little change at any dosing velocity and reach approximately H_g/h = 1.5 in the equilibrium state. However, the case C40-C40 appears to have a dependency on the dosing velocity. The thickness of the gel layer

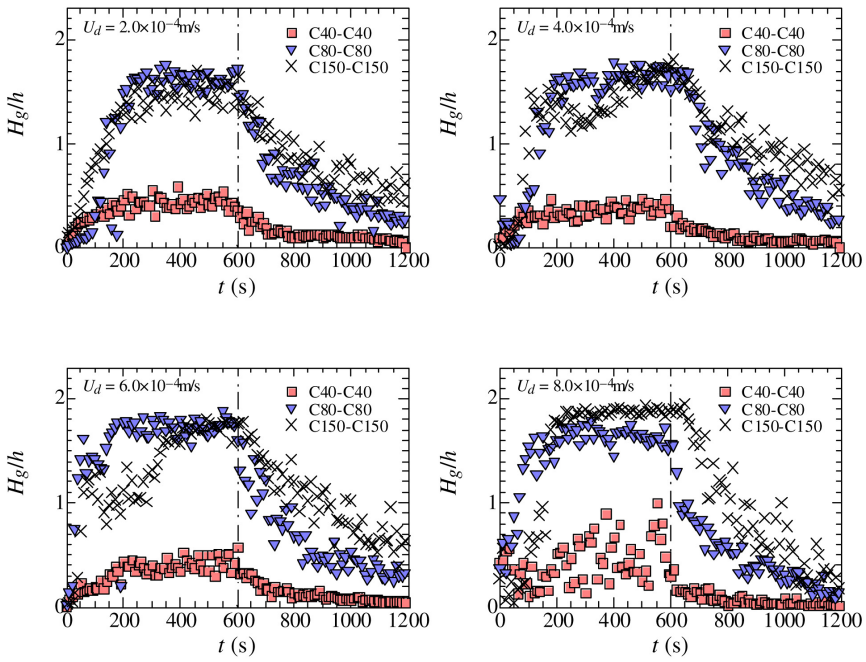

Figure 5. Dosing time dependency of the thickness of the gel-like SIS layer for different dosing velocities.

reaches a steady state at approximately $H_g/h = 0.5$. In the case of a low surfactant concentration condition, because the strength of the gel layer is low, the destruction rate and the growth rate are balanced when the gel layer occupies one-fourth of the channel full width, and the remainder is the flow region.

5. Boundary Conditions on Gel-Like SIS Layer

Pressure loss measurement was performed to bridge the corresponding relation of the blocking situation and the boundary condition of the stress on the gel-like SIS layer. The pump driving the channel flow was operated at a constant speed during the solution dosing, and as the gel layer thickness changed, the flow rate varied and the pressure loss tended to increase. The measured pressure loss, L, is normalized by the dynamic pressure of the channel flow, calculated from U_b and the fluid density, ρ. The transition of the pressure loss with time during and after the termination of dosing is displayed in Figure 6. The dosing is also stopped at $t = 600$ s. In the case of C25-C25, the trend of the pressure loss remains relatively small and steady, despite the starting of the dosing. It is also slightly decreased after the dosing is stopped. The values are almost unchanged at all the dosing velocities. From the visualization, this case does not exhibit gel formation regardless of the dosing conditions, and the pressure loss is nearly unchanged.

However, for the cases of high-surfactant concentration conditions, C40-C40, C80-C80, and C150-C150, the pressure loss continues to increase after the dosing is started and reaches up to approximately ten times than that at the starting dosing. In comparison with the thickness of the gel-like SIS layer, the channel flow is restricted as the gel layer develops, and the pressure loss of the channel flow also increases. In particular, the pressure loss in the cases of C80-C80 and

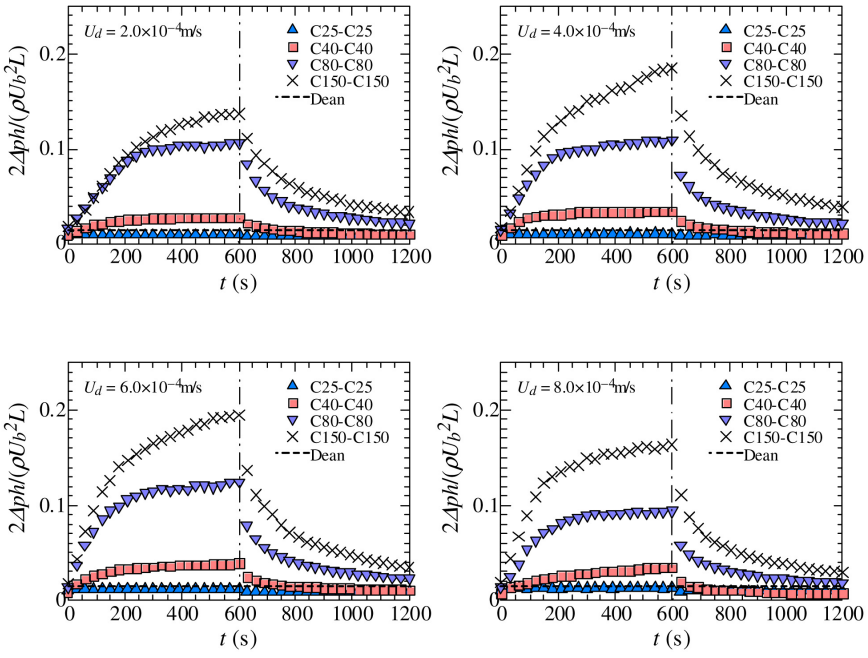

Figure 6. Dosing time dependency of the pressure loss for various dosing velocities.

C150-C150 increases rapidly after the dosing is started, and subsequently the increasing rate decreases. In the transition of the gel thickness with time, the thickness is obtained from the local image at the measurement position, as displayed in Figure 5. This thickness fluctuates owing to the undulation of the gel layer. Therefore, we cannot confirm the accurate time when the increase in the thickness decreases under certain conditions because of the large scatter of the plot. However, the pressure loss is related to the integral of the friction force between the measuring taps, and results with less scatter are obtained. The time variation of the pressure loss is similar to the temporal transition of the thickness of the gel layer obtained by image analysis. There is a strong correlation between the restriction of the channel flow and the increase in the pressure loss due to the growth of the gel-like SIS layer.

In the high-surfactant concentration case, the strength of the gel-like SIS layer rises and overcomes its destruction by the stress, and hence a thicker gel layer grows. Consequently, the channel flow is restricted with a large pressure loss. The gel layer can support the force from the pressure gradient up to approximately 20% of the dynamic pressure. Therefore, it can be inferred that there is a phenomenon in which a dilute solution, which is originally a fluid state, causes remarkable solid formation only by passing through the permeable wall and by the change in the state by an elongation deformation.

6. Effect of Elongational Deformation on the Thickness of Gel-Like SIS Layer

It was found that a gel-like SIS layer could be formed by dosing the surfactant solution through the permeable wall, as explained in the previous section. As the gel layer develops, the flow region on the gel layer becomes narrower, so that the shear stress acting on the surface of the gel layer increases. Further, the pressure loss increases accordingly. As the gel layer thickness reaches equilibrium with the shear stress on the surface, the strength of the gel is related to the thickness of the gel layer. In this study, we discuss the influence of the dosing conditions on the thickness of the layer.

In the present study, the Reynolds number of the channel flow is fixed at 1.0×10^4 and the thickness of the gel layer reaching equilibrium H_{gm} was compared. The maximum thickness, H_{gm}, was calculated for each case of surfactant concentration and dosing velocity by averaging the values obtained from the image analysis at the time of 500 - 600 s in which the equilibrium state is considered. The dosing from the permeable wall imposes a strong elongation on the solution as it passes through the layered wire mesh, which may promote a strong gel formation in the thread shape [13]. The flow passing through the opening of the wire mesh on the surface is elongated when passing through the opening of the wire mesh. Therefore, the dosing velocity is converted to the elongation rate by a simple model, *i.e.*, elongation rate $\dot{\varepsilon} = \left(U_d - U_0\right)/0.5d$, where U_d is the dosing velocity, U_0 is the velocity before passing through the mesh, and d is the diameter of the mesh wire on the permeable wall facing the channel flow. However,

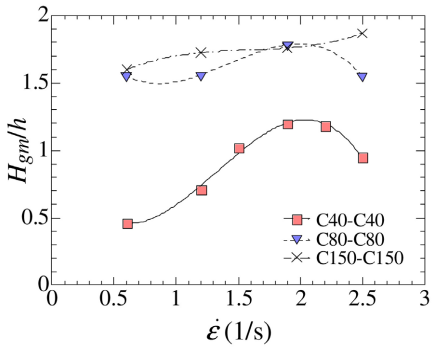

Figure 7. Elongational rate dependency of the maximum thickness of the gel-like SIS layer H_{gm}.

because the permeable wall in this experiment is obtained by sintering a seven-wire mesh with various wire diameters and openings, this conversion is effective only to find a qualitative tendency. The elongation rate dependency of the maximum thickness of the gel layer, H_{gm}, is displayed in **Figure 7**. For the cases of C80-C80 and C150-C150, the gel thickness has little dependence on the elongation and is always maintained over $1.5h$. For the case of C40-C40, the value initially increases and subsequently decreases as the elongation rate increases; however, it is lower than those in the cases of C80-C80 and C150-C150. The dependency of the gel strength on the elongation rate can be understood from the viewpoint that SIS is formed at a critical deformation rate. Although the gel-like SIS formation is not sufficiently performed at a low elongation rate, the excessive deformation causes the breaking of the gel-like SIS at a high elongation rate and leads to the weak strength of the gel.

7. Conclusions

The present study aimed to characterize the gel-like shear-induced structure (SIS) formation for dosing a surfactant solution into the channel flow from the permeable wall attached to a side wall. This provides elongation and shear deformation to the solution. The permeable wall was composed of sintered wire mesh layers. We performed pressure loss measurements, PIV, and PLIF measurements for various combinations of the channel flow fluid and the dosing fluid. A fluorescent dye was added to the dosing fluid for generating fluorescence video images; therefore, so we detected areas having a high brightness and identify the dosing fluid area marked by the dye. The acquisition of the images was started simultaneously with the start of dosing, and the acquisition was continued for some time even after the dosing was stopped. These tests were performed to investigate the conditions for forming a gel-like SIS, a transition of differential pressure loss, growth, and destruction of the gel layer.

In the PLIF visualization, by dosing a dilute surfactant solution through the wire mesh, a white striped area was observed, which largely covered the wire mesh plate. This area had a zero streamwise mean velocity and vibrates, but it remained stuck to the wall. As the mean lateral flow was present outside the

layer, the shear stress existed in the white area despite no flow, and therefore, it is considered that the white area behaves as a soft solid and a lump of the gel sticky on the wire mesh wall. Thus, we determined this white striped area as the gel-like SIS layer.

From the time-lapse observation of the PIV images and pressure loss, we observed the transition of the gel thickness with time and the restriction process on the channel. After gradually growing the gel-like SISs, the growth stopped owing to the increase in the stress acting on the upper surface of the gel-like SIS. The gel-like SIS layer grew rapidly even in the turbulent flow and reached the equilibrium thickness. After the termination of the dosing, the gel layer collapsed gradually. In addition, because the thickness of the gel-like SIS layer strongly depended on the surfactant concentration and the elongation rate in the wire mesh, it was found that the strength of the gel changed depending on the surfactant concentration and the dosing rate.

The present study successfully demonstrates the formation of gel layers on the order of 10 mm thick in turbulent channel flow by the slow dosing of a dilute surfactant solution. This result suggests a new cost-effective manufacturing route for soft materials with high biocompatibility. In future work, it is desirable to investigate the gel formation phenomena for a nonionic surfactant of a much more biocompatible solution. For the application of this gel, to avoid the use of a potentially harmful gelator, a syringe with meshes to enable the gel in the blood to flow in the heart and in the main blood vessels would be useful for cellular or drug delivery with high retention capacity and sustained release. Furthermore, we expect that this sol-gel transition deployed on a large scale can be helpful in various techniques such as sensing and for use in gel valves capable of autonomous control of local flow and in machine elements for motion resembling the organism in terms of biomimetics.

Conflicts of Interest

The authors declare no conflicts of interest regarding the publication of this paper.

References

[1] Suzuki, A. and Tanaka, T. (1990) Phase Transition in Polymer Gels Induced by Visible Light. *Nature*, **346**, 345-347. https://doi.org/10.1038/346345a0

[2] Kwon, I.C., Bae, Y.H. and Kim, S.W. (1991) Electrically Erodible Polymer Gel for Controlled Release of Drugs. *Nature*, **354**, 291-293. https://doi.org/10.1038/354291a0

[3] Osada, Y., Okuzaki, H. and Hori, H. (1992) A Polymer Gel with Electrically Driven Motility. *Nature*, **355**, 242-244. https://doi.org/10.1038/355242a0

[4] Chen, G. and Hoffman, A.S. (1995) Graft Copolymers that Exhibit Temperature-Induced Phase Transitions over a Wide Range of pH. *Nature*, **373**, 49-52. https://doi.org/10.1038/373049a0

[5] Stayton, P.S., Shimoboji, T., Long, C., Chilkoti, A., Ghen, G., Harris, J.M. and

Hoffman, A.S. (1995) Control of Protein-Ligand Recognition Using a Stimuli-Responsive Polymer. *Nature*, **378**, 472-474. https://doi.org/10.1038/378472a0

[6] Miyata, T., Asami, N. and Uragami, T. (1999) A Reversibly Antigen-Responsive Hydrogel. *Nature*, **399**, 766-769. https://doi.org/10.1038/21619

[7] Palleau, E., Morales, D., Dickey, M.D. and Velev, O.D. (2013) Reversible Patterning and Actuation of Hydrogels by Electrically Assisted Ionoprinting. *Nature Communications*, **4**, Article No. 2257. https://doi.org/10.1038/ncomms3257

[8] Liu, C.H. and Pine, D.J. (1996) Shear-Induced Gelation and Fracture in Micellar Solutions. *Physical Review Letters*, **77**, 2121-2124. https://doi.org/10.1103/PhysRevLett.77.2121

[9] Chu, Z. and Feng, Y. (2010) Amidosulfobetaine Surfactant Gels with Shear Banding Transitions. *Soft Matter*, **6**, 6065-6067. https://doi.org/10.1039/c0sm00874e

[10] Yamamoto, T., Sawa, K. and Mori, K. (2009) Velocity Measurements for Shear Flows of CTAB/NaSal Aqueous Solutions between Parallel Plates. *Journal of Rheology*, **53**, 1347-1362. https://doi.org/10.1122/1.3216942

[11] Mitishita, R.S., Elfring, G.J. and Frigaard, I.A. (2022) Turbulent Drag Reduction of Viscoelastic Wormlike Micellar Gels. *Journal of Non-Newtonian Fluid Mechanics*, **301**, Article ID: 104724. https://doi.org/10.1016/j.jnnfm.2021.104724

[12] Tuan, N.A., Kobayashi, Y. and Mizunuma, H. (2017) Turbid and Transparent Shear-Induced Structures in Dilute Cationic Surfactant Solutions. *Journal of Rheology*, **61**, 83-91. https://doi.org/10.1122/1.4967955

[13] Vasudevan, M., Buse, E., Lu, D., Krishna, H., Kalyanaraman, R., Shen, A.Q., Khomami, B. and Sureshkumar, R. (2010) Irreversible Nanogel Formation in Surfactant Solutions by Microporous Flow. *Nature Materials*, **9**, 436-441. https://doi.org/10.1038/nmat2724

[14] Cheung, P., Dubash, N. and Shen, A.Q. (2012) Local Micelle Concentration Fluctuations in Microfluidic Flows and its Relation to a Flow-Induced Structured Phase (FISP). *Soft Matter*, **8**, 2304-2309. https://doi.org/10.1039/c2sm06772b

[15] Cardiel, J.J., Dohnalkova, A.C., Dubash, N., Zhao, Y., Cheung, P. and Shen, A.Q. (2013) Microstructure and Rheology of a Flow-Induced Structured Phase in Wormlike Micellar Solutions. *Proceedings of the National Academy of Sciences of the United States of America*, **404**, E1653-E1660. https://doi.org/10.1073/pnas.1215353110

[16] Khan, A., Khan, D., Khan, I., Ali, F., Karim, U.F. and Imran, M. (2018) MHD Flow of Sodium Alginate-Based Casson Type Nanofluid Passing Through a Porous Medium with Newtonian Heating. *Scientific Reports*, **8**, Article No. 8645. https://doi.org/10.1038/s41598-018-26994-1

[17] Nisar, S.K., Khan, D., Khan, A., Khan, W.A, Khan, I. and Aldawsari, A.M. (2019) Entropy Generation and Heat Transfer in Drilling Nanoliquids with Clay Nanoparticles. *Entropy*, **21**, Article No. 1226. https://doi.org/10.3390/e21121226

[18] Ling, S.C. and Ling, T.Y.J. (1974) Anomalous Drag-Reducing Phenomenon at a Water/Fish-Mucus or Polymer Interface. *Journal of Fluid Mechanics*, **65**, 499-512. https://doi.org/10.1017/S0022112074001509

[19] Pasquali, M. (2004) Polymer Composites: Swell Properties and Swift Processing. *Nature Materials*, **3**, 509-510. https://doi.org/10.1038/nmat1188

[20] Joshi, A., Punyani, S., Bale, S.S., Yang, H., Borca-Tasciuc, T. and Kane, R.S. (2008) Nanotube-Assisted Protein Deactivation, *Nature Nanotechnology*, **3**, 41-45. https://doi.org/10.1038/nnano.2007.386

[21] Pasquali, M. (2010) Grow with the Flow. *Nature Materials*, **9**, 381-382. https://doi.org/10.1038/nmat2761

[22] Tiederman, W.G., Luchik, T.S. and Bogard, D.G. (1985) Wall-Layer Structure and Drag Reduction. *Journal of Fluid Mechanics*, **156**, 419-437. https://doi.org/10.1017/S0022112085002178

[23] Usui, H., Maeguchi, K. and Sano, Y. (1988) Drag Reduction Caused by the Injection of Polymer Thread into a Turbulent Pipe Flow. *The Physics of Fluids*, **31**, 2518-2523. https://doi.org/10.1063/1.866605

[24] Walker, D.T. and Tiederman, W.G. (1990) Turbulent Structure in a Channel Flow with Polymer Injection at the Wall. *Journal of Fluid Mechanics*, **218**, 377-403. https://doi.org/10.1017/S0022112090001045

[25] Tamano, S. Uchikawa, H., Ito, J. and Morinishi, Y. (2018) Streamwise Variations of Turbulence Statistics up to Maximum Drag Reduction State in Turbulent Boundary Layer Flow due to Surfactant Injection. *Physics of Fluids*, **30**, Article ID: 075103. https://doi.org/10.1063/1.5036589

[26] Beebe, D.J., Moore, J.S., Bauer, J.M., Yu, Q., Liu, R.H., Devadoss, C.L. and Jo, B.H. (2000) Functional Hydrogel Structures for Autonomous Flow Control inside Microfluidic Channels. *Nature*, **404**, 588-590. https://doi.org/10.1038/35007047